Adaptive Optimal Control of Faulty Nonlinear DC Microgrids with Constant Power Loads: Dual-Extended Kalman Filter Approach

Navid Vafamand, Mohammad Mehdi Arefi, *Senior Member, IEEE,* Miadreza Shafie-khah, *Senior Member, IEEE,* and João P. S. Catalão, *Fellow, IEEE*[1]

***Abstract*—This article investigates the problem of estimating actuator fault and states and controlling the bus voltage in direct current microgrids (DC MGs) with linear and nonlinear constant power loads (CPLs). It is considered that the DC MG states are not fully measurable and the utilized sensors are not ideal and noisy. Additionally, the actuator fault occurs and it is modeled as an additive term in the power system dynamics. These issues, including nonlinearities, un-measurable states, noisy measures, and actuator fault indispensably degrade the operation of the DC MG. To solve this issue, initially, a dual-extended Kalman filter (dual-EKF) is suggested for the fault and state estimation. It decomposes the process of estimating the state and actuator fault to reduce the online computational burden. For the control purpose, a linear parameter varying (LPV) model predictive control (MPC) is suggested to regulate the current and voltage of the DC MG. It benefits the nonlinear system modeling of LPV representation and constrained-based design procedure of the MPC to result in an accurate and low online computational burden dealing with system constraints. By deploying the overall robust adaptive dual-EKF estimation-based LPV-MPC, there is no need to have any prior knowledge of all system states and actuator faults in prior. The theoretical analysis and controller design are validated by numerical simulations on a typical islanded DC MG and comparisons are done with state-of-the-art estimation and control strategies.**

***Index Terms*—DC microgrid, constant power load, actuator fault, dual-extended Kalman filter, linear parameter varying representation, nonlinear model predictive control.**

Navid Vafamand and Mohammad Mehdi Arefi are with the Department of Power and Control Engineering, School of Electrical and Computer Engineering, Shiraz, Iran, Email: {n.vafamand , arefi}@shirazu.ac.ir.

Miadreza Shafie-khah is with the School of Technology and Innovations, University of Vaasa, Vaasa, Finland, Email: mshafiek@uwasa.fi.

João P. S. Catalão is with the Faculty of Engineering of the University of Porto (FEUP) and INESC TEC, Porto 4200-465, Portugal (Email: catalao@fe.up.pt).

NOMENCLATURE

A. DC microgrid parameters

R	Load resistance
P	CPL power
C	Converter capacitance
L	Converter inductance
V_e	Source voltage
$x_1 = v_c$	Capacitor voltage
$x_2 = i_L$	Inductor current
u	Converter duty cycle
f_a	Actuator fault

B. Dual-extended Kalman filter parameters

v_x (v_f)	State (fault) system noise
Q_x (Q_f)	State (fault) system variance
$\hat{x}$ ($\hat{f}$)	Estimation of state (fault)
P_x (P_f)	Variance of state (fault) estimation
K_x (K_f)	State (fault) Kalman gain

C. LPV-MPC parameters

θ_1 (θ_2)	Lower (upper) bound of local region
σ_1 and σ_2	Slopes of sectors
β_1 and β_2	LPV time-varying parameters
$\xi_{\max}$ ($\xi_{\min}$)	Upper (lower) bound of control input
J	Cost function
σ and λ	Weights of cost function
w	Sequence of future reference
U	Sequence of future control inputs

I. INTRODUCTION

Direct current (DC) microgrids (MGs) facilitate transmitting and distributing DC power from distributed generation units, renewable energy sources, and energy storage devices to flexible DC loads. These small-scale MGs are becoming popular, because of high robustness, modest control, and desired proficiency in integrating DC sources such as photovoltaics and fuel cells [1].

Despite their merits, the DC MGs face three main challenging issues:

i) DC MGs feed nonlinear constant power loads (CPLs), which can destabilize the DC MG by inserting a negative incremental resistant [2], [3].

ii) Practical DC MGs are not fully observable, as they require too many voltage and current sensors. Besides, the installed sensors are also not ideal and subjected to noise, which reduces the measurement reliability.

iii) The controllable power electronic devices deployed in DC MGs may be subjected to faults that degrade the performance.

The above-mentioned challenges influence the DC MG power system operation and must be considered in designing monitors and controllers. A few control and/or estimation approaches have been conducted to deal with these issues.

The stability margin of DC MGs with CPLs is enhanced by active stabilizing techniques with linear and nonlinear control strategies [4], [5]. In contrast to linear control laws, such as the well-known proportional-integral (PI) and proportional-integral-derivative (PID), nonlinear and advanced control approaches, including sliding mode [6], [7], backstepping [8], [9], and predictive [10], [11], result into global stabilization for the DC MG. Nevertheless, nonlinear controllers, which deploy Lyapunov stability to guarantee stability, need the information of the power system state vector in their laws. Thereby, they are commonly vulnerable to faults and/or noisy measurements.

For the DC MG power systems subjected to a fault, some detection methods classified into data-driven and model-based methods are presented [12]. Compared to the former group, the latter classification has a lower online computational burden and a higher robustness level against noise. A high-gain Luenberger observer is designed based on the linearized representation of the nonlinear DC MGs with CPLs in [13]. By using the difference between the actual and estimation of the measurement output, a systemic approach to determine faults is presented. Nevertheless, faults are not reconstructed and the state vector is not estimated, accurately. In [14], a fusion mechanism to integrate the estimations of Kalman filters is presented to isolate the faulty sensors and determine the estimations precisely. Nevertheless, faults are not reconstructed. Sensor faults detection and state estimation can be utilized to monitor a power system. But high-performance control actions rely on detecting and reconstructing actuator faults to compensate for them. In [15], the actuator and sensor faults were detected by developing a robust linear observer. However, the detected faults were not estimated. In [16], the issue of sensor and actuator faults for DC MGs with CPLs is solved by suggesting a Takagi-Sugeno fuzzy sliding mode observer. Nevertheless, the approach of [16] is applicable if some matrix rank conditions hold and transformations are found. This limits that approach's applicability in facing complicated DC MGs.

In [1], the dual-EKF approach is adopted and applied to the DC MG power system with a pre-given converter duty cycle. Although actuator faults are reconstructed in [1], the fault-tolerant control (FTC) of nonlinear DC MGs is not addressed.

The occurring generator faults in an aircraft are detected and mitigated by a robust monitoring and controller technique in [17]. In [18], a hybrid AC/DC MG with faulty conditions is regulated by a passivity-based FTC approach. The common drawback of [17] and [18] is the lack of reconstructing actual faults and they are only tolerated. In [19], a typical DC MG with CPLs and several faults is considered and an FTC method is presented. Since CPL is controlled by an FTC, the overall FTC method of [19] is not suitable for complicated DC MGs with a high number of CPLs. Analyzing state-of-the-art methods determines that most of the control methods for DC MGs with CPLs are not robust against actuator faults or necessitate a complicated online implementation.

This work develops a novel robust adaptive LPV-MPC for the class of islanded nonlinear DC MGs with noisy measurements and actuator faults. The main novelty of this work is deploying the instantaneous information of the actuator fault in the control law. The actuator fault as well as the system states are estimated online by a novel dual-extended Kalman filter (dual-EKF) method. By using the dual-EKF, not only the issue of actuator fault in the power system is involved to make the estimations more accurate, but also the actuator faults are precisely constructed. Then, all estimated information is deployed in the nonlinear LPV-MPC to optimally design the duty cycle of the DC/DC converter such that it regulates the voltage and current of the DC MG. The optimal control law is computed online in the presence of power system constraints. Since the DC MG with CPL and DC/DC converter is nonlinear, both the estimator and controller are nonlinear and effective in the presence of nonlinearity to assure large-signal stability. In this regard, the dual-EKF uses two separate EKFS applicable to nonlinear system dynamics. Also, the predictive controller is integrated with nonlinear LPV representation to improve the prediction action. The proposed approach is validated by performing numerical simulations. Several scenarios and comparative results are presented to demonstrate the advantages of the estimation and control methods.

This article is continued as follows. In Section II, the dynamics of a typical DC MG with a buck converter, CPLs, linear loads, and actuator fault are presented. In Section III, the proposed dual-EKF-based LPV-MPC is discussed. In Section IV, comparative simulations are given and the results are discussed. In Section V, this work achievement is summarized and future works to extend the presented results are suggested.

II. Faulty DC MG with CPLs

Typical DC MGs connect several energy sources, such as renewable, fully controllable, and storage to a wide variety of linear and nonlinear loads. These loads can be DC or AC and connected to the main bus via DC/DC converters or DC/AC inverters. A simplified DC MG is illustrated in Fig. 1. If the power electronic apparatus exactly regulates the receiving power to the loads, they act as nonlinear CPLs.

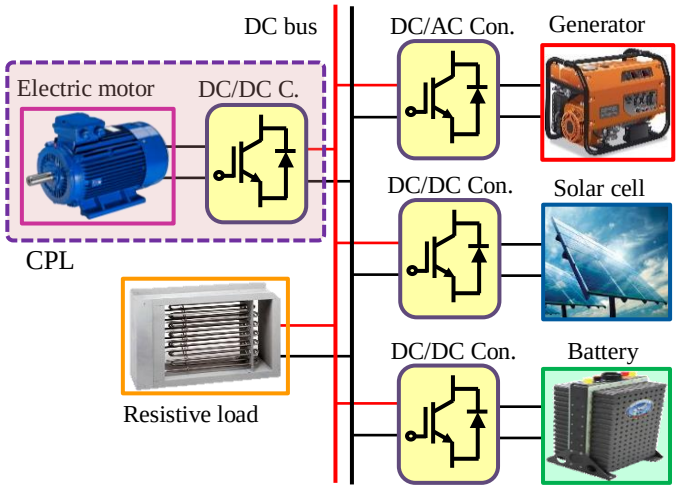

Fig. 1. DC MG system illustration.

Without loss of generality, by incorporating all energy sources to construct a common fixed voltage source, using the Thevenin-Norton theorem of the resistive loads at the DC side, and considering CPLs' behavior at the input of converter or inverters connected to the DC side, a simplified DC MG schematic is achieved in Fig. 2. More precisely, it is assumed that the power generators are controlled properly and so their combination is simplified and results in a constant voltage level. The constant power source is connected to the DC bus via a buck converter, which should be controlled. Moreover, loads may operate at different voltage levels and should be connected to the DC bus via converters and inverters. By the means of the Thevenin-Norton theorem, their equivalent values are added to simplify the DC MG.

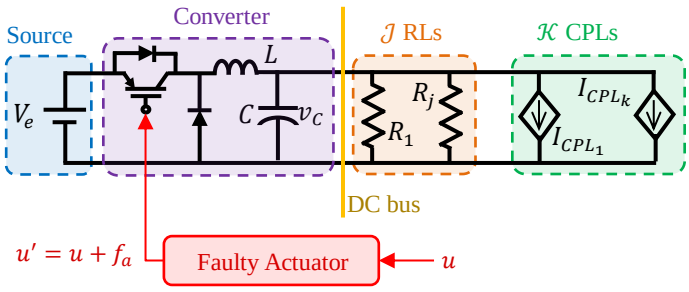

Fig. 2. DC MG power system structure.

This DC MG connects a DC source to $\mathcal{K}$ CPLs, and $\mathcal{J}$ RLs via a controllable DC/DC converter. Whereas the CPLs P_{CPL_s} for $s = 1, \dots, \mathcal{K}$ and resistive loads R_s for $s = 1, \dots, \mathcal{J}$ are in parallel, they can be further simplified by a common resistive load (i.e. R) and CPL (i.e. P), as shown in (1) and (2).

$$R = \left(R_1^{-1} + \cdots + R_{\mathcal{J}}^{-1}\right)^{-1}, P = P_{CPL_1} + \cdots + P_{CPL_{\mathcal{K}}}. \quad (1)$$

The switching nature of the DC/DC buck converter can be described by an averaged model of the duty cycle in the interval $0 \le u \le 1$. It is considered that the controllable DC/DC converter may operate with faults. This fault arises from any mal-functionality of power electronic devices. This influences the control command and degrades the closed-loop DC MG performance. Reminding (1) and involving the effect of fault on the controllable converter, the nonlinear averaged state-space representation for the DC MG of Fig. 2 can be obtained. Although the power converter behaves switch, based on some circumstances, the switching actions of the buck converter can be smoothed by a duty cycle and the overall power system is represented by an averaged model. As stated in [20], the averaged modeling method has high accuracy, if the natural frequency of the converter filter is much lower than that of the switching action. The dynamics of the DC MG power system are as follows:

$$\begin{cases} \dot{x}_1 = \dfrac{1}{C}x_2 - \dfrac{x_1}{RC} - \dfrac{P}{Cx_1} \\ \dot{x}_2 = \dfrac{V_e}{L}u - \dfrac{1}{L}x_1 + \dfrac{V_e}{L}f_a \\ y = x_1 \end{cases}. \quad (2)$$

Where $x_1 = v_c$ and $x_2 = i_L$ are first state (capacitor voltage) and second state (inductor current), and f_a is the actuator fault. The capacitance and inductance are C and L, respectively and V_e is the source voltage. As can be seen in (2), the measured state is x_1.

It is worth noting that the dynamics (2) are derived by considering the following assumptions:

I) The DC/DC buck converter is modeled by the averaged model and its command input is the duty cycle.
II) The source has a fixed voltage.
III) The CPLs are modeled by current-controlled sources, which their current is related to their voltages and the constant power.
IV) The additive term actuator fault is represented by an unknown input that appears in the model equation.

Moreover, the additive fault and disturbances have a similar influence on the system [21]. The main difference is that disturbance inputs are known to exist. But faults should be detected. actuator fault is modeled as an additive term. Dealing with fault has two main steps [21]. I) Initially, the fault should be detected and the detection procedure should be robust against disturbance inputs to avoid wrong alarm. II) After a correct fault detection, fault reconstruction should be performed to monitor the system and control it. The focus of this work is on the second step of the fault-tolerant controller design.

The key objective for the DC MG system (2) is to regulate the DC bus voltage in the presence of the actuator fault. In this regard, let the desired voltage reference be x_1^*. Therefore, the desired value for the inductor current and converter duty cycle in the fault-free environment can be calculated by letting $\dot{x}_1 = 0$, $\dot{x}_2 = 0$, and $f_a = 0$, as follows:

$$x_2^* = \frac{x_1^*}{R} + \frac{P}{x_1^*}, u^* = \frac{x_1^*}{V_e}. \quad (3)$$

Applying the change of variables $\tilde{x}_1 = x_1 - x_1^*$, $\tilde{x}_2 = x_2 - x_2^*$, and $\tilde{u} = u - u^*$, the dynamics (2) can be rewritten as follows:

$$\begin{cases} \dot{\tilde{x}}_1 = \dfrac{1}{C}\tilde{x}_2 - \dfrac{\tilde{x}_1}{RC} - \dfrac{P\tilde{x}_1}{C(\tilde{x}_1 + x_1^*)x_1^*} \\ \dot{\tilde{x}}_2 = \dfrac{V_e}{L}\tilde{u} - \dfrac{1}{L}\tilde{x}_1 + \dfrac{V_e}{L}f_a \\ \tilde{y} = \tilde{x}_1 \end{cases}. \quad (4)$$

Now, the control objective is to force the tracking errors in the dynamics (4) to reach zero. The dynamics (4) are continuous-time and have a nonlinear term $h(\tilde{x}_1) = \tilde{x}_1/(\tilde{x}_1 + x_1^*)$, which complicates the design of the controller. To avoid such complexities, the representation is discretized by the forward Euler method, as follows:

$$\dot{\tilde{x}}_i(t_0) = \lim_{T\to 0} \frac{\tilde{x}_i(t_0+T) - \tilde{x}_i(t_0)}{T} \cong \frac{\tilde{x}_i(t_0+T) - \tilde{x}_i(t_0)}{T}. \quad (5)$$

Where T is the discretizing sample. By setting the instance $t_k = t_0 + kT$ with t_0 is the initial time, one step of the Euler method from t_k to t_{k+1} will be $t_{k+1} = t_k + T$. For simplicity, define the time instances t_k and t_{k+1} as k and $k+1$, respectively. Thereby, (4) is discretized as follows:

$$\begin{cases} \tilde{x}_1(k+1) = \tilde{x}_1(k) + T\left(\dfrac{\tilde{x}_2(k)}{C} - \dfrac{\tilde{x}_1(k)}{RC} + \dfrac{P\tilde{x}_1(k)}{C(\tilde{x}_1(k) + x_1^*)x_1^*}\right) \\ \tilde{x}_2(k+1) = \tilde{x}_2(k) + T\left(\dfrac{V_e}{L}\tilde{u}(k) - \dfrac{1}{L}\tilde{x}_1(k) + \dfrac{V_e}{L}f_a(k)\right) \end{cases}. \quad (6)$$

Furthermore, the nonlinear term $h(\tilde{x}_1) = \tilde{x}_1/(\tilde{x}_1 + x_1^*)$ should be represented by an equivalent polytopic-LPV representation. The way of deriving the polytopic-LPV model is based on the sector nonlinearity method [22]. In this method, for each nonlinear term, two sectors are defined such that the nonlinear term is within those sectors. Then, based on the sectors, the polytopic-LPV model can be obtained. It is worth noting that generally, nonlinear terms are within two linear sectors. In this case, the sectors are selected in a local region. For the local region $\mho = \{\tilde{x}_1 | -x_1^* < \theta_1 \le \tilde{x}_1 \le \theta_2\}$, the nonlinear term is within two sectors $\sigma_1 x_2$ and $\sigma_2 x_2$, as shown in Fig. 3.

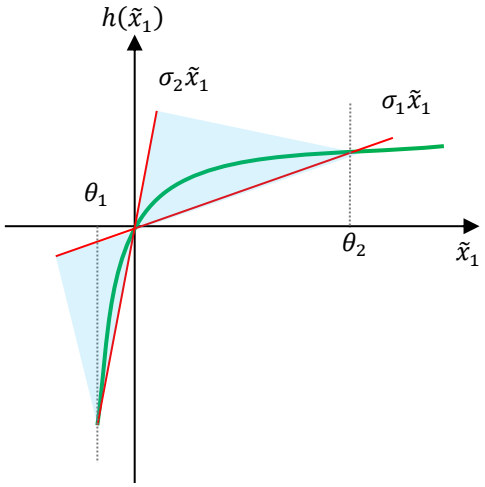

Fig. 3. Sector region of the nonlinear term $h(\tilde{x}_1) = \tilde{x}_1/(\tilde{x}_1 + x_1^*)$.

For the region $\mho = \{\tilde{x}_1 | -x_1^* < \theta_1 < \tilde{x}_1 < \theta_2\}$, the slopes σ_1 and σ_2 are calculated as follows:

$$\sigma_1 = \frac{1}{\theta_2 + x_1^*}; \sigma_2 = \frac{1}{\theta_1 + x_1^*}. \quad (7)$$

Reminding the sector nonlinearity approach, the nonlinear term $h(\tilde{x}_1)$ is represented as follows:

$$h(\tilde{x}_1) = \beta_1\sigma_1\tilde{x}_1 + \beta_2\sigma_2\tilde{x}_1. \quad (8)$$

Where $\beta_1 + \beta_2 = 1$, and:

$$\beta_1 = \frac{\sigma_2\tilde{x}_1 - h(\tilde{x}_1)}{(\sigma_2 - \sigma_1)\tilde{x}_1}, \beta_2 = \frac{h(\tilde{x}_1) - \sigma_1\tilde{x}_1}{(\sigma_2 - \sigma_1)\tilde{x}_1}. \quad (9)$$

Substituting (8) into (4) results in a 2-vertex polytopic LPV model, as follows:

$$\left\{\tilde{x}(k+1) = \sum_{i=1}^{2} \beta_i\{A_i\tilde{x} + B_1\tilde{u} + B_1 f_a\}. \right. \quad (10)$$

Where $\tilde{x} = [\tilde{x}_1 \;\; \tilde{x}_2]^T$ and:

$$A_1 = \begin{bmatrix} 1 - \dfrac{T}{RC} + \dfrac{TP\sigma_1}{Cx_1^*} & \dfrac{T}{C} \\ -\dfrac{T}{L} & 1 \end{bmatrix}, A_2 = \begin{bmatrix} 1 - \dfrac{T}{RC} + \dfrac{TP\sigma_2}{Cx_1^*} & \dfrac{T}{C} \\ -\dfrac{T}{L} & 1 \end{bmatrix},$$

$$B_1 = \begin{bmatrix} 0 \\ \dfrac{TV_e}{L} \end{bmatrix}.$$

Comparing the dynamics (6) and (10) reveals that the polytopic-LPV model comprises linear state-space models $A_i\tilde{x} + B_1\tilde{u} + B_1 f_a$, which are aggregated with nonlinear scalars β_i. Thanks to this structure of polytopic-LPV system, it is possible to use linear control methods for nonlinear systems. In the following, a novel nonlinear control law is proposed for the power system case study.

III. Dual EKF-based LPV-MPC Controller

A common way of dealing with nonlinearities in the power system is to use a Lipchitz-based MPC [23]. However, the conservativeness increases. Another and improved method is by using the discrete-time LPV representation (10), a polytopic LPV-MPC with a finite-time prediction can be designed. The dynamics (10) consider the fault term f_a, which future value is not known in practice. Its future values can be assumed to be constant and its present value can be considered as a biased term. In this regard, the polytopic LPV-MPC design approach of [24] is applicable. The following theorem provides the LPV-MPC control design procedure.

Theorem 1 (Polytopic LPV-MPC) [24]. Consider the polytopic LPV system:

$$\begin{cases} x(k+1) = \sum_{i=1}^{r} \beta_i A_i x(k) + \sum_{i=1}^{r} \beta_i B_i u(k) + \sum_{i=1}^{r} \beta_i E_i \\ \qquad = A_\beta x(k) + B_\beta u(k) + E_\beta \\ y(k) = \sum_{i=1}^{r} \beta_i C_i x(k) = C_\beta x(k) \end{cases}, \quad (11)$$

and the input constraint:

$$\xi_{\min}(.) < u(.) < \xi_{\max}(.), \tag{12}$$

and the cost function over the finite-time prediction and control intervals N_p and N_u:

$$J(N_p, N_u) = \sum_{j=1}^{N_p} \delta(j)[\hat{y}(k+j|k) - w(k+j)]^2 + \sum_{j=1}^{N_u} \lambda(j)[u(k+j-1)]^2. \tag{13}$$

Where $\hat{y}(k+j|k)$ is the j-step ahead prediction of the output, $w(k+j)$ is the future reference, and $\delta(j)$ and $\lambda(j)$ are coefficients of the tracking error and the energy effort.

The following LMI-based optimization problem assures the sub-optimum solution of the LPV-MPC controller:

$$min\ J^*$$

subject to:

$$\begin{bmatrix} J^* - G - K^T U + U^T K^T & U^T \\ U & H^{-1} \end{bmatrix} > 0 \tag{14}$$

$$\begin{bmatrix} I \\ -I \end{bmatrix} U < \begin{bmatrix} \Xi_{max} \\ -\Xi_{\min} \end{bmatrix} \tag{15}$$

Where:

$$\Theta = \begin{bmatrix} C_\beta B_\beta & \dots & 0 \\ C_\beta A_\beta B_\beta & \dots & 0 \\ \vdots & \ddots & \vdots \\ C_\beta A_\beta^{N_p-1} B_\beta & \dots & C_\beta A_\beta^{N_p-N_u} B_\beta \end{bmatrix},$$

$$\Psi = \begin{bmatrix} C_\beta A_\beta \\ \vdots \\ C_\beta A_\beta^{N_p} \end{bmatrix} x(k) + \begin{bmatrix} C_\beta \\ C_\beta(I + A_\beta) \\ \vdots \\ \sum_{i=0}^{N_p-1} C_\beta A_\beta^i \end{bmatrix} E_\beta,$$

$$H = \Theta^T \Delta \Theta + \Lambda, K = (\Psi - W)^T \Delta \Theta, \tag{16}$$

$$G = (\Psi - W)^T \Delta (\Psi - W),$$

$$W = \begin{bmatrix} w(t+1) & w(t+2) & \dots & w(t+N_p) \end{bmatrix}^T,$$

$$\Delta = \text{diag}\{\delta(1), \delta(2), \dots \delta(N_p)\},$$

$$\Lambda = \text{diag}\{\lambda(1), \lambda(2), \dots, \lambda(N_p)\},$$

$$U = [u(k)\ \ u(k+1)\ \dots\ u(k+N_u-1)]^T,$$

$$\Xi_{max} = [\xi_{max}(k), \dots, \xi_{max}(k+N_u)]^T,$$

$$\Xi_{min} = [\xi_{min}(k), \dots, \xi_{min}(k+N_u)]^T,$$

and diag{.} is the diagonal matrix, and I is the identity matrix.

As can be seen in Theorem 1, the system (11) contains a biased term E_β and its value affects the control law based on (24). Besides the controller law use the information of the state vector $x(k)$.

Reminding that the control objective for the tracking error dynamics (10) is to stabilize the error states to zero, to apply Theorem 1 on the power system dynamics (10), it should be considered in (11) that:

$$E_\beta = B_1 f_a, C_\beta = I, W = 0. \tag{17}$$

Using Theorem 1, the future sequence of control input U is calculated online and the present control input is the first array of U, (i.e. $\tilde{u}(k) = U(1)$). On the other hand, the actuator fault and the whole states are not measurable in practice, because they require several sensors to be installed. Therefore, it is logical to estimate the power system states and actuator fault. Among all possible deterministic and stochastic nonlinear estimators, in this paper, the dual-EKF algorithm is deployed. The algorithm for implementing the LPV-MPC of Theorem 1 is given in Fig. 4.

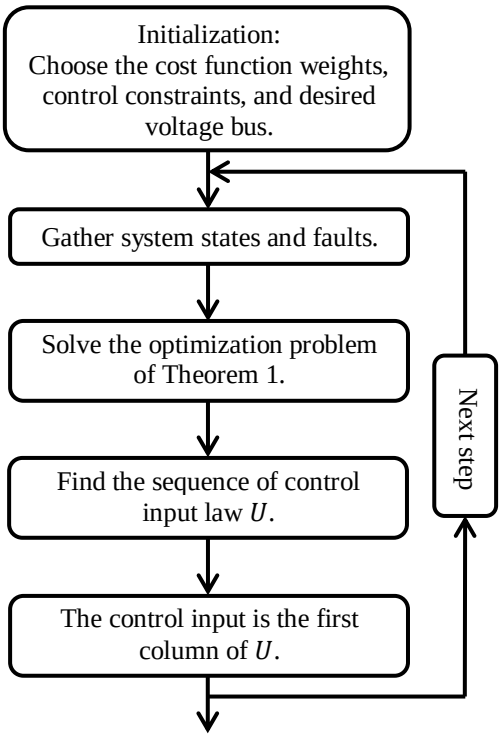

Fig. 4. LPV-MPC implementation.

The dual-EKF algorithm is systematic and highly robust against noisy measurements and mildly robust against system parameters and unknown dynamics. It also outperforms the accuracy and computational burden of a conventional EKF, by using two EKFs that estimate the state vector and actuator faults in parallel [25], [26]. To deal with the estimation issue of the actuator fault f_a in (10), its dynamic is required. Though in practice, fault behavior cannot be explicitly modeled and the time-derivative of the actuator fault is not known. Therefore, it is considered that:

$$f_a(k+1) = f_a(k). \tag{18}$$

The relation (18) assumes that the actuator fault is constant, which is in harmony with the LPV-MPC controller. As considered

in (17), it is assumed that in the instance of design of the control law, the actuator fault behaves constantly to predict the future system behavior.

To develop the dual-EKF, which is based on a Jacobian matrix, the dynamics (10) and (18) are augmented and represented as follows:

$$\begin{cases} \begin{bmatrix} \tilde{x}(k+1) \\ f_a(k+1) \end{bmatrix} = \begin{bmatrix} \Psi_{xx}(k) & \Psi_{xf} \\ \Psi_{fx} & \Psi_{ff} \end{bmatrix} \begin{bmatrix} \tilde{x}(k) \\ f_a(k) \end{bmatrix} \\ \qquad\qquad + \begin{bmatrix} B_x \\ B_f \end{bmatrix} u(k) + \begin{bmatrix} v_x(k) \\ v_f(k) \end{bmatrix}. \\ y(k) = [C_x \quad 0] \begin{bmatrix} \tilde{x}(k) \\ f_a(k) \end{bmatrix} + w(k) \end{cases} \tag{19}$$

Where $v(k) = \left[v_x^T(k), v_f^T(k)\right]^T$ and $w(k)$ are Gaussian white noises $\mathcal{g}$ standing for the system and measurement noises, respectively, characterized by with mean vector and variance matrix, as follows:

$$\begin{bmatrix} v_x(k) \\ v_f(k) \end{bmatrix} \sim \mathcal{g}\left(0, \begin{bmatrix} Q_x & 0 \\ 0 & Q_f \end{bmatrix}\right) \tag{20}$$

$$w(k) \sim \mathcal{g}(0, R_w) \tag{21}$$

Also, the Jacobian matrices are as follows:

$$\begin{gathered} \Psi_{xx}(k) = \begin{bmatrix} 1 + \frac{-T}{RC} + \frac{PT}{C(\tilde{x}_1(k)+x_1^*)^2} & \frac{T}{C} \\ -\frac{T}{L} & 1 \end{bmatrix}, \Psi_{xf} = \begin{bmatrix} 0 \\ \frac{TV_e}{L} \end{bmatrix}, \\ \Psi_{ff} = 1, \ \Psi_{fx} = [0 \ \ 0], B_x = \left[0 \ \ \frac{TV_e}{L}\right]^T, B_f = 0, \\ C_x = [1 \quad 0]. \end{gathered} \tag{22}$$

Based on the augmented Jacobian matrix-based state-space representation (19), the following algorithm summarizes the dual-EKF implementation.

Algorithm 1 (Dual-EKF) [1]: The dual-EKF algorithm comprises an offline initialization and online recursive parts:

1. Initialize the state and actuator fault filters' parameters.

$$\hat{x}^+(0), P_x^+(0), \tag{23}$$

$$\hat{f}^+(0), P_f^+(0), \frac{\partial \hat{x}^+(0)}{\partial f}. \tag{24}$$

Where $\hat{x}^+(.)$ and $\hat{f}^+(.)$ are the estimations of the states $\tilde{x}(.)$ and $f_a(.)$, $P_x^+(.)$ and $P_f^+(.)$ are the covariance matrices of the estimation errors, and $\frac{\partial \hat{x}^+(.)}{\partial f}$ is the interaction of the filters.

2. Update the state and actuator fault filter with respect to time.

$$\begin{cases} \hat{x}^-(k) = \Psi_{xx}(k)\hat{x}^+(k-1) \\ P_x^-(k) = \Psi_{xx}(k)P_x^+(k-1)\Psi_{xx}^T(k) + Q_x \end{cases}, \tag{25}$$

$$\begin{cases} \hat{f}^-(k) = \Psi_{ff}\hat{f}^+(k-1) \\ P_f^-(k) = \Psi_{ff}P_f^+(k-1)\Psi_{ff}^T + Q_f \\ \frac{\partial \hat{x}^-(k)}{\partial f} = \Psi_{xx}(k)\frac{\partial \hat{x}^+(k-1)}{\partial f} + \Psi_{xf} \end{cases}. \tag{26}$$

3. Update the state and actuator fault filter with respect to measurement.

$$\begin{cases} K_x(k) = P_x^-(k)C_x^T(C_xP_x^-(k)C_x^T + R_w)^{-1} \\ \hat{x}^+(k) = \hat{x}^-(k) + K_x(k)(y(k) - C_x\hat{x}_k^-) \\ P_x^+(k) = (I - K_x(k)C_x)P_x^-(k) \end{cases}, \tag{27}$$

$$\begin{cases} K_f(k) = P_x^-(k)C_f^T\left(C_fP_f^-(k)C_f^T + R_w\right)^{-1} \\ \hat{f}^+(k) = \hat{f}^-(k) + K_f(k)(y(k) - C_x\hat{x}_k^-) \\ P_f^+(k) = \left(I - K_f(k)C_f\right)P_f^-(k) \\ \frac{\partial \hat{x}^+(k)}{xf} = (I - K_x(k)C_x)\frac{\partial \hat{x}^-(k)}{xf} \end{cases}. \tag{28}$$

Where the artificial fault output matrix C_f is as follows:

$$C_f = C_x\frac{\partial \hat{x}^+(k-1)}{\partial xf}. \tag{29}$$

4. Let $k = k + 1$ and go to Step 3.

As mentioned before, the dual-EKF uses two parallel filters to estimate the states and actuator fault. In Algorithm 1, the details of implementing these two filters are given. However, they can operate in parallel, based on Fig. 5. As can be seen in Fig. 5, two parallel filters are performed and the algorithms of the time update and measurement update are separated into two parts, each of which is used in each filter. Now, based on Theorem 1 and Algorithm 1, the closed-loop system schematic is obtained in Fig. 6. The DC MG power system dynamics (2) are considered as the open-loop system. The system output and control inputs are used in the dual-EKF to estimate the state vector and actuator faults. The dual-EKF uses Algorithm 1 based on the flowchart of Fig. 5 to calculate the estimation $\hat{x}(k)$ and $\hat{f}_a(k)$. Then, the LPV-MPC computes the control law by using Theorem 1 and the optimization problem (14)-(16) is implemented based on Fig. 4.

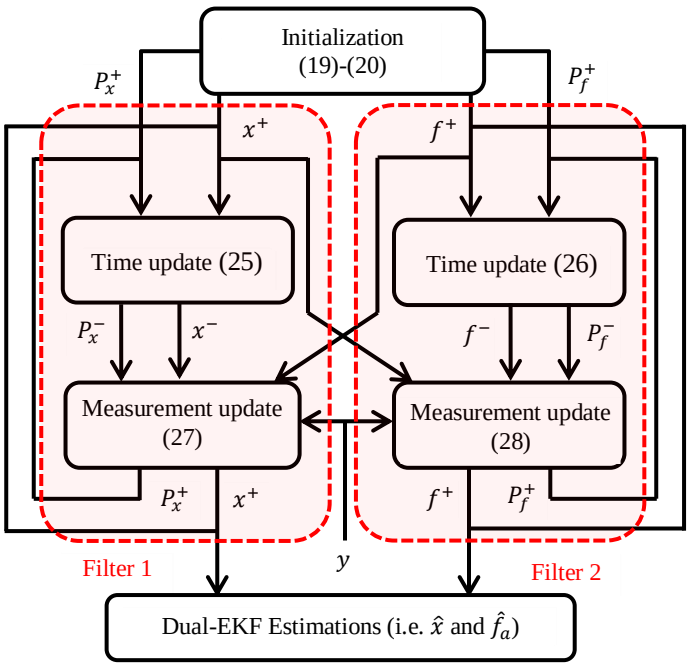

Fig. 5. Dual-Kalman filter algorithm.

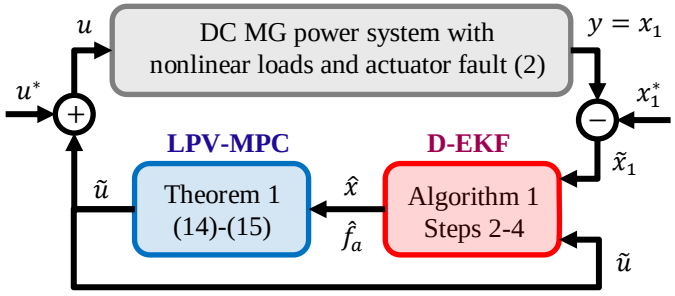

Fig. 6. Implementation of the proposed estimation method.

It should be noted that the actual states and control input of the power system (i.e. x and u) differ from those of the dual-EKF and LPV-MPC (i.e. $\tilde{x}$ and $\tilde{u}$ in (6)). Therefore, changes of variables (3) (i.e. $\tilde{x}_1 = x_1 - x_1^*$ and $u = \tilde{u} + u^*$) are required to construct the closed-loop system.

Due to appearing actuator fault and input constraints, the proposed controller uses the dual-EKF and an online LPV-MPC. The dual-EKF is capable of decomposing the state and fault estimation procedures. Therefore, when a fault is detected, then the whole dual-EKF should be implemented; and when the fault is not detected, only the EKF of the state estimation should be performed. Besides, by implementing the separate EKFs by two digital processors, the overall online calculation time decreases. Although the DC MG power system is nonlinear, the online optimization problem of the LPV-MPC is solved by LMIs, which use convex optimization with low online calculations. Therefore, the proposed approach requires a low online computational burden compared to the available online nonlinear observer-based controllers.

IV. Simulation Results

The DC MG power system dynamics (2) of Fig. 2 with the parameter values $R = 10\ (\Omega)$, $C = 500\ (\mu F)$, $L = 39.5\ (mH)$, $P = 300\ (W)$, and $V_e = 200\ (V)$ are considered. The measurement of the case study in Fig. 2 is the bus voltage. The system is discretized with the sampling time is $T = 1\ (msec)$ and the output measurement noise variance is $R_w = 0.1$. Two scenarios are considered to evaluate the performance of the dual-EKF and the LPV-MPC approach. The results are compared with state-of-the-art methods.

Scenario 1 (Evaluating the Dual-EKF performance):

Since the goal of this scenario is to evaluate the performance of the state and actuator estimator, the duty cycle of the DC/DC buck converter is set as $u = 0.5$. Initially, the power system without actuator fault is simulated and the applicability of the dual-EKF is compared with the conventional EKF and UKF. The key difference between the EKF and UKF is the way of approximating the nonlinearities. In the EKF, the nonlinearity terms are linearized at each step, meanwhile, the UKF uses the so-called sigma points to compute the state vector mean value and estimation variance matrix. These algorithms are considered for comparison to show how the dual-EKF outperforms the EKF and UKF when faults occur. The details of the EKF and UKF algorithms can be found in [27].

The initial conditions of the dual-EKF are given in Table I.

TABLE I. Initial Conditions of the Dual-EKF

State filter
$\hat{x}^+(0) = [130, 10]^T$, $P_x^+(0) = 10^3 I$, $Q_x = 10^{-3} I$
Fault filter
$\hat{f}^+(0) = 0$, $P_f^+(0) = 10^2$, $\frac{\partial \hat{x}^+(0)}{\partial f} = [0, 0]^T$, $Q_f = 10^{-5}$

Table II illustrates the computational burden and estimation precision of both considered filters.

TABLE II. Performance Comparison of Dual-EKF, EKF, and UKF

	Dual-EKF	EKF	UKF
Mean value of the computational burden (seconds)	1.95 $\times 10^{-4}$	1.14 $\times 10^{-4}$	7.85 $\times 10^{-4}$
Norm 2 of the voltage estimation error	20.9638	21.0625	14.0457
The voltage maximum steady-state error (volts)	0.3987	0.3975	0.7706
Norm 2 of the current estimation error	8.0936	8.2180	2.1943
The current maximum steady-state error (amperes)	0.1932	0.1940	0.5075

The computational burden of the dual-EKF is calculated for that Algorithm 1, which is implemented with one processor. If two parallel processors implement the dual-EKF, then the mean value of the computation time burden reduces to 11.4017 milliseconds, which is almost similar to the conventional EKF time of 11.4012 milliseconds. From another point of view, the dual-EKF slightly provides more precise estimations than the conventional EKF for steady-state errors and norms 2. Besides, the UKF has the highest online computational burden, due to computing sigma points and propagating the mean vector and covariance matrices. The UKF results in smaller norm 2 of estimation errors, which indicates that system and measurement noises are better mitigated compared to the EKF and dual-EKF. On the other hand, the maximum steady-state values of the estimation errors of the UKF are higher than those based on the EKF and dual-EKF. Thereby, the UKF reacts to the estimations error slower and with higher overshoot than the other methods.

In the next study, the following time varying actuator fault is considered:

$$f_a = 0.2 \sin(4/3\pi t). \tag{30}$$

A time-varying actuator fault can be more challenging than a constant value because, in (18) and thus the dual-EKF formulation, it is assumed that a fault is constant. By adding the actuator fault (30) and setting a constant duty cycle for the converter (i.e. $u = 0.5$), the DC MG power system states behave in an oscillatory way, as shown in Fig. 7.

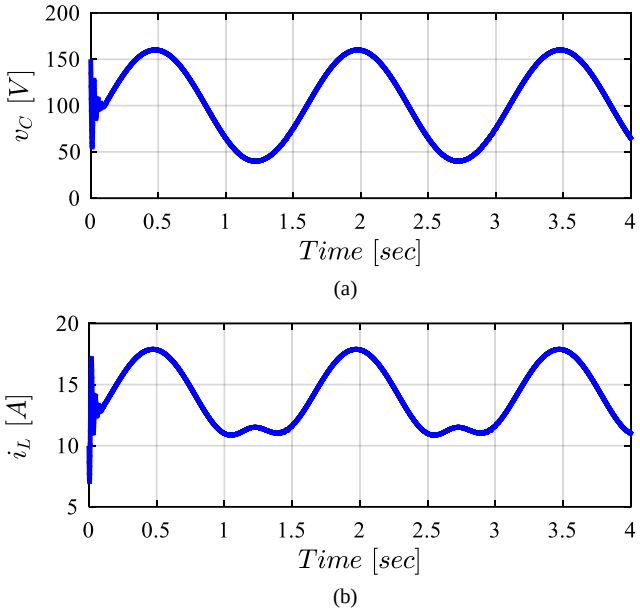

Fig. 7. The DC MG power system states in the presence of the actuator fault: **(a)** $x_1 = v_C$, **(b)** $x_2 = i_L$.

The estimation errors of the power system states and actuator fault based on the dual-EKF and EKF are plotted in Fig. 8. Both approaches accurately estimate $x_1 = v_c$, because this state is measurable via a noisy sensor. Since its correct but noisy value is available, the filters only try to decompose noise. The estimation errors of the state $x_2 = i_L$ based on the conventional EKF are high. Additionally, the UKF results in a very high biased error and it is not plotted in Fig 8. Because the conventional EKF and UKF fail to estimate actuator fault and cannot compensate for its effects on the estimation errors. Theoretically, the conventional EKF and UKF methods lead to unbiased estimation, when the actuator fault is not involved. However, the actuator fault appears, since its expected value is not zero, the estimations are biased. On the other hand, the dual-EKF algorithm involves the actuator fault in its estimation process and provides unbiased estimations.

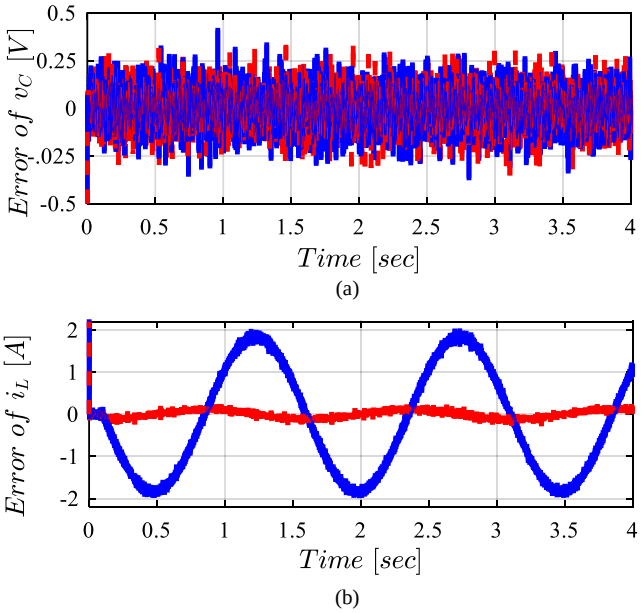

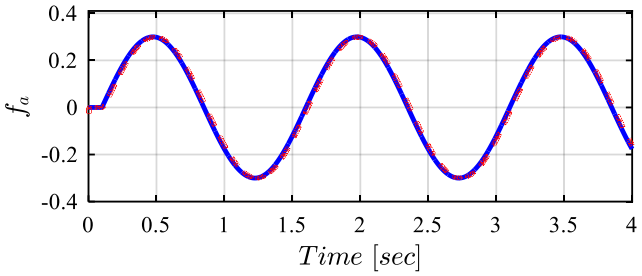

Fig. 8. Estimation error (Dual-EKF by the red line and EKF by the blue line): **(a)** voltage estimation, **(b)** current estimation, **(c)** actuator fault estimation.

Reminding Fig. 8(b) shows that by using the conventional EKF, the second state is estimated with about 11.7% error. On the other hand, the dual-EKF not only accurately estimates the second state but also constructs the actuator fault in Fig. 8(c). Thus, the dual-EKF successfully determines the effects of the actuator fault. It is worth noting that the considered actuator fault f_a changes in the range $[-0.3, 0.3]$, and the duty cycle control input varies in the range $[0,1]$. This shows that the considered actuator fault amplitude is 30% of the control input and changes the DC bus voltage ± 60 volts.

Scenario 2 (Evaluating the dual-EKF-based LPV-MPC performance):

In this scenario, the effectiveness of the proposed overall controller is evaluated for the power system with the actuator fault of Fig. 9(a).

The cost function weights of the LPV-MPC are set as $\delta(\cdot) = \lambda(\cdot) = 1$. Also, the control input amplitude constraint is set as $\xi_{max} = 1$ and $\xi_{min} = 0$.

The actuator fault comprises stepwise and sinusoidal functions. Also, the desired reference for the DC bus voltage is $x_1^* = 128\,[V]$. For comparison, the closed-loop system with constant control input $u = 0.5$ and the approach EKF-MPC approach [28] are considered. That approach uses the original nonlinear system instead of tracking error dynamics. Therefore, the future reference for the states is chosen based on (3).

The closed-loop DC bus voltages based on the considered control methods are provided in Fig. 9(b). Fig. 9(b) reveals that although these approaches stabilize the DC MG, there is a steady-state error based on the approach [28]. Moreover, Fig. 9(c) illustrates that based on the proposed approach, the current of the converter has less oscillation than the other control methods, which is consistent with the fixed DC bus voltage in Fig. 9(b). The main advantage of the proposed approach over [28] is that the information of the actuator fault is utilized to predict the future behavior of the power system, which makes it robust against faults. This results in an accurate voltage regulation based on the proposed approach. Besides, the proposed approach considers the amplitude constraints of the duty cycle, which is not the case in [28].

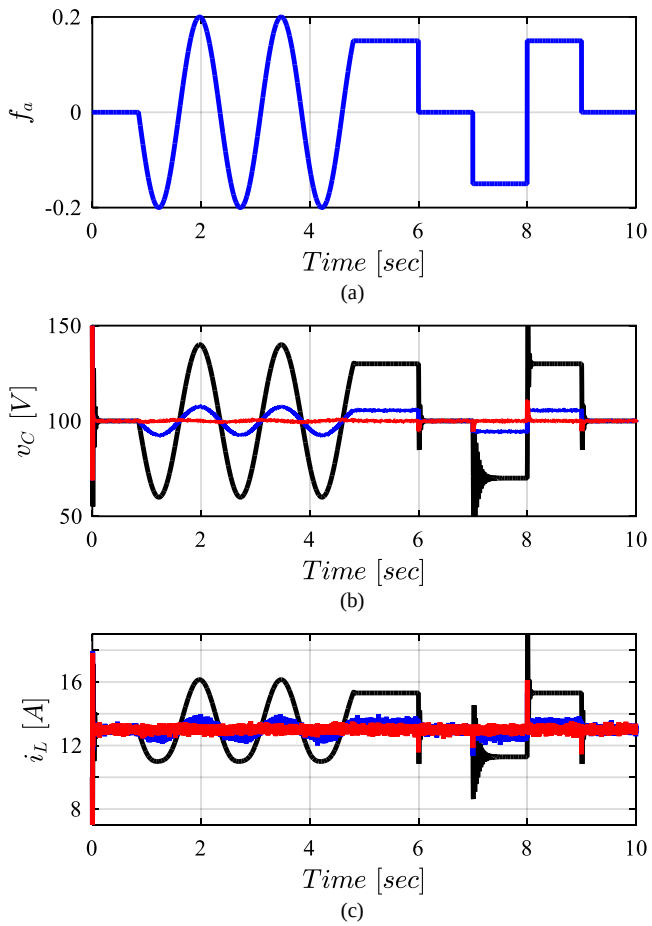

Fig. 9. The actuator fault and DC bus voltage in Scenario 2 (No control by the black line, proposed approach by the red line, and the MPC [28] by the blue line): **(a)** f_a, **(b)** x_1, **(c)** x_2.

Additionally, to illustrate the closed-loop stability of the power system, based on the online LPV-MPC, the logarithmic value of the cost function (13) is given in Fig. 10. As can be seen in Fig. 10, the cost function decreases, expect the instances that faults change, suddenly. Since the cost function can be regarded as a Lyapunov candidate and is decreasing, closed-loop system stability is assured. It is worth noting that due to the noisy measurements, the predictions of the system output experience some oscillations.

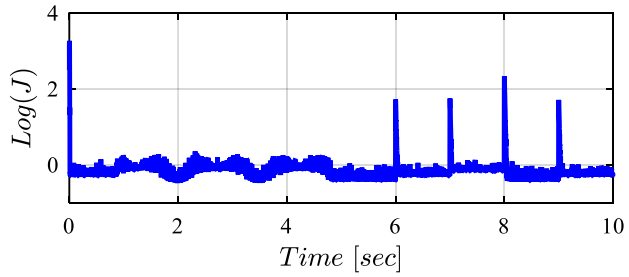

Fig. 10. The logarithmic value of the cost function (13).

V. Conclusion

This article investigated the issue of state and actuator fault estimation and adaptive controller design for faulty DC MG power systems with nonlinear CPLs. A novel robust nonlinear adaptive controller based on LPV representation, constrained model predictive schematic, and dual-EKF approach was suggested for the power system. The proposed approach has some advantages listed as follows: i) The LPV representation provides a systematic method to predict the future behavior of the power system as a linear function of future control inputs. Thus, the online computational burden decreases; ii) On the other hand, occurring actuator faults affect the power system and by regarding it as a biased term, MPC was considered; iii) The value of the actuator fault was estimated by the dual-EKF. In the dual-EKF, two EKFs were combined, each of which estimates the system states and the actuator fault. Decomposing these two EKFs in the dual-EKF reduces the online implementation of the estimator. The improvement of the dual-EKF LPV-MPC over the conventional EKF-MPC was shown in the numerical simulations. It was shown that the conventional nonlinear Kalman filters such as EKF and UKF fail to estimate the current of DC MG correctly, as it neglected the actuator fault. Also, using that inaccurate estimation in the MPC leads to regulation error. Moreover, the dual-EKF estimates all states and actuator fault, and therefore, using their information in the LPV-MPC with bias term stabilizes the power system precisely. For future work, these topics are advised: i) considering power system uncertainties and developing a robust Kalman filter; ii) evaluating the effect of different kinds of faults; iii) using the proposed approach to distributed DC MGs.

References

[1] N. Vafamand, M. M. Arefi, M. Shafie-khah, and J. P. S. Catalao, "Estimating Faults in Nonlinear DC Microgrids with Constant Power Loads: A Dual-Extended Kalman Filter Approach," in *2021 IEEE International Conference on Environment and Electrical Engineering and 2021 IEEE Industrial and Commercial Power Systems Europe (EEEIC / I&CPS Europe)*, Bari, Italy, Sep. 2021, pp. 1–6. doi: 10.1109/EEEIC/ICPSEurope51590.2021.9584736.

[2] M. N. Hussain, R. Mishra, and V. Agarwal, "A Frequency-Dependent Virtual Impedance for Voltage-Regulating Converters Feeding Constant Power Loads in a DC Microgrid," *IEEE Trans. Ind. Appl.*, vol. 54, no. 6, pp. 5630–5639, Nov. 2018, doi: 10.1109/TIA.2018.2846637.

[3] M. A. Kardan *et al.*, "Improved Stabilization of Nonlinear DC Microgrids: Cubature Kalman Filter Approach," *IEEE Trans. Ind. Appl.*, vol. 54, no. 5, pp. 5104–5112, Sep. 2018, doi: 10.1109/TIA.2018.2848959.

[4] M. M. Namazi, H. R. Koofigar, and J.-W. Ahn, "Active Stabilization of Self-Excited Switched Reluctance Generator Supplying Constant Power Load in DC Microgrids," *IEEE J. Emerg. Sel. Top. Power Electron.*, vol. 9, no. 3, pp. 2735–2744, Jun. 2021, doi: 10.1109/JESTPE.2020.2994017.

[5] S. Ansari, J. Zhang, and R. E. Singh, "A review of stabilization methods for DCMG with CPL, the role of bandwidth limits and droop control," *Prot. Control Mod. Power Syst.*, vol. 7, no. 1, p. 2, Dec. 2022, doi: 10.1186/s41601-021-00222-x.

[6] B. A. Martinez-Trevino, A. E. Aroudi, A. Cid-Pastor, G. Garcia, and L. Martinez-Salamero, "Synthesis of Constant Power Loads Using Switching Converters Under Sliding-Mode Control," *IEEE Trans. Circuits Syst. Regul. Pap.*, vol. 68, no. 1, pp. 524–535, Jan. 2021, doi: 10.1109/TCSI.2020.3031332.

[7] C. Zheng, T. Dragicevic, J. Zhang, R. Chen, and F. Blaabjerg, "Composite Robust Quasi-Sliding Mode Control of DC–DC Buck Converter With Constant Power Loads," *IEEE J. Emerg. Sel. Top. Power Electron.*, vol. 9, no. 2, pp. 1455–1464, Apr. 2021, doi: 10.1109/JESTPE.2020.3021942.

[8] H. Amiri, G. A. Markadeh, and N. M. Dehkordi, "Voltage control in a DC islanded microgrid based on nonlinear disturbance observer with CPLs," *J. Energy Storage*, vol. 29, p. 101296, Jun. 2020, doi: 10.1016/j.est.2020.101296.

[9] X. Li, X. Zhang, W. Jiang, J. Wang, P. Wang, and X. Wu, "A Novel Assorted Nonlinear Stabilizer for DC–DC Multilevel Boost Converter With Constant

Power Load in DC Microgrid," *IEEE Trans. Power Electron.*, vol. 35, no. 10, pp. 11181–11192, Oct. 2020, doi: 10.1109/TPEL.2020.2978873.

[10] F. Naseri, E. Farjah, Z. Kazemi, E. Schaltz, T. Ghanbari, and J.-L. Schanen, "Dynamic Stabilization of DC Traction Systems Using a Supercapacitor-Based Active Stabilizer With Model Predictive Control," *IEEE Trans. Transp. Electrification*, vol. 6, no. 1, pp. 228–240, Mar. 2020, doi: 10.1109/TTE.2020.2964423.

[11] Z. Karami, Q. Shafiee, Y. Khayat, M. Yaribeygi, T. Dragicevic, and H. Bevrani, "Decentralized Model Predictive Control of DC Microgrids With Constant Power Load," *IEEE J. Emerg. Sel. Top. Power Electron.*, vol. 9, no. 1, pp. 451–460, Feb. 2021, doi: 10.1109/JESTPE.2019.2957231.

[12] N. Bayati, H. R. Baghaee, A. Hajizadeh, and M. Soltani, "Localized Protection of Radial DC Microgrids With High Penetration of Constant Power Loads," *IEEE Syst. J.*, vol. 15, no. 3, pp. 4145–4156, Sep. 2021, doi: 10.1109/JSYST.2020.2998059.

[13] K. Jessen, M. Soltani, and A. Hajizadeh, "Sensor Fault Detection for Line Regulating Converters supplying Constant Power Loads in DC Microgrids," in *2020 IEEE 11th International Symposium on Power Electronics for Distributed Generation Systems (PEDG)*, Dubrovnik, Croatia, Sep. 2020, pp. 99–103. doi: 10.1109/PEDG48541.2020.9244467.

[14] A. Vafamand, B. Moshiri, and N. Vafamand, "Fusing Unscented Kalman Filter to Detect and Isolate Sensor faults in DC Microgrids with CPLs," *IEEE Trans. Instrum. Meas.*, 2021.

[15] A. Salimi, Y. Batmani, and H. Bevrani, "Model-Based Fault Detection in DC Microgrids," in *2019 Smart Grid Conference (SGC)*, Tehran, Iran, Dec. 2019, pp. 1–6. doi: 10.1109/SGC49328.2019.9056589.

[16] S. Asadi, N. Vafamand, M. Moallem, and T. Dragicevic, "Fault Reconstruction of Islanded Nonlinear DC Microgrids: An LPV-based Sliding Mode Observer Approach," *IEEE J. Emerg. Sel. Top. Power Electron.*, pp. 1–1, 2020, doi: 10.1109/JESTPE.2020.3043491.

[17] R. Todd and A. J. Forsyth, "DC-bus power quality for aircraft power systems during generator fault conditions," *IET Electr. Syst. Transp.*, vol. 1, no. 3, p. 126, 2011, doi: 10.1049/iet-est.2010.0056.

[18] M. Davari, W. Gao, and F. Blaabjerg, "A Fault-Tolerant, Passivity-Based Controller Enhanced by the Equilibrium-to-Equilibrium Maneuver Capability for the DC-Voltage Power Port VSC in Multi-Infeed AC/DC Modernized Grids," *IEEE J. Emerg. Sel. Top. Power Electron.*, vol. 8, no. 3, pp. 2484–2507, Sep. 2020, doi: 10.1109/JESTPE.2019.2917650.

[19] P. Magne, B. Nahid-Mobarakeh, and S. Pierfederici, "A design method for a fault-tolerant multi-agent stabilizing system for DC microgrids with Constant Power Loads," in *2012 IEEE Transportation Electrification Conference and Expo (ITEC)*, Dearborn, MI, USA, Jun. 2012, pp. 1–6. doi: 10.1109/ITEC.2012.6243469.

[20] G. W. Wester and R. D. Middlebrook, "Low-Frequency Characterization of Switched dc-dc Converters," *IEEE Trans. Aerosp. Electron. Syst.*, vol. AES-9, no. 3, pp. 376–385, May 1973, doi: 10.1109/TAES.1973.309723.

[21] M. Blanke and J. Schröder, Eds., *Diagnosis and fault-tolerant control*, 2nd ed. Berlin ; New York: Springer, 2006.

[22] K. Tanaka, *Fuzzy control systems design and analysis: a linear matrix inequality approach*. New York: Wiley, 2001.

[23] I. Hosseini, S. V. Naghavi, and A. A. Safavi, "Distributed Model Predictive Control Strategy for a Class of Interconnected Discrete-Time Systems with Communication Delay," *Iran. J. Sci. Technol. Trans. Electr. Eng.*, vol. 43, no. 2, pp. 267–276, Jun. 2019, doi: 10.1007/s40998-018-0085-1.

[24] N. Vafamand, M. M. Arefi, M. H. Khooban, T. Dragicevic, and F. Blaabjerg, "Nonlinear Model Predictive Speed Control of Electric Vehicles Represented by Linear Parameter Varying Models with Bias terms," *IEEE J. Emerg. Sel. Top. Power Electron.*, vol. 74, pp. 134–143, 2018, doi: 10.1109/JESTPE.2018.2884346.

[25] E. A. Wan and A. T. Nelson, "Dual Kalman filtering methods for nonlinear prediction, smoothing, and estimation," *Adv. Neural Inf. Process. Syst.*, vol. 9, pp. 793–799, 1997.

[26] H. Khodadadi and H. Jazayeri-Rad, "Applying a dual extended Kalman filter for the nonlinear state and parameter estimations of a continuous stirred tank reactor," *Comput. Chem. Eng.*, vol. 35, pp. 2426–2436, 2011.

[27] D. Simon, *Optimal state estimation: Kalman, H∞ and nonlinear approaches*. Hoboken, N.J: Wiley-Interscience, 2006.

[28] S. Yousefizadeh, J. D. Bendtsen, N. Vafamand, M. H. Khooban, T. Dragičević, and F. Blaabjerg, "EKF-based Predictive Stabilization of Shipboard DC Microgrids with Uncertain Time-varying Loads," *J. Emerg. Sel. Top. Power Electron.*, 2018.